Neutron-powder-diffraction study of the nuclear and magnetic structures of the substitution compound $(Y_{1-x}Ca_x)Ba_2Fe_3O_{8+\delta}$ ($x=0.05$, 0.10, and 0.20)

I. Natali Sora
Reactor Radiation Division, National Institute of Standards and Technology, Gaithersburg, Maryland 20899

Q. Huang
University of Maryland, College Park, Maryland 20742
and Reactor Radiation Division, National Institute of Standards and Technology, Gaithersburg, Maryland 20899

J. W. Lynn and N. Rosov
Reactor Radiation Division, National Institute of Standards and Technology, Gaithersburg, Maryland 20899

P. Karen and A. Kjekshus
Department of Chemistry, University of Oslo, Blindern, N-0315 Oslo, Norway

V. L. Karen, A. D. Mighell, and A. Santoro*
Reactor Radiation Division, National Institute of Standards and Technology, Gaithersburg, Maryland 20899
(Received 23 August 1993)

The nuclear and magnetic structures of $(Y_{1-x}Ca_x)Ba_2Fe_3O_{8+\delta}$ with $x=0.05$, 0.10, and 0.20 have been investigated by neutron-powder diffraction at room temperature. The compound crystallizes with the symmetry of space group $P4/mmm$ and has a structure similar to that of the superconductor $YBa_2Cu_3O_7$ (1:2:3). There are two types of Fe atoms in the unit cell, one having fivefold pyramidal coordination and the other octahedral coordination. The Ca and Y atoms are randomly distributed over the $\frac{1}{2},\frac{1}{2},\frac{1}{2}$ position, which are exclusively occupied by Y in the 1:2:3 superconductor. Since the oxygen sites on the basal plane of the structure are fully occupied to achieve octahedral coordination for the iron atoms on this plane, the oxygen content is eight atoms per formula unit, the barium atoms are twelvefold coordinated, and the coordination polyhedron is a cuboctahedron. Extra oxygen atoms corresponding to $\delta=0.08$ and 0.05 are located in the Y/Ca layer. The presence of these atoms produces disorder in the structure resulting in a shift of the oxygen atoms located near the plane of the pyramidal iron atoms. The charge compensation required by the substitution of Y^{3+} by Ca^{2+} is achieved in these materials by elimination of the extra oxygen, rather than oxidation of the iron atoms. The magnetic structure is based on a unit cell related to that of the nuclear structure by the transformation of axes $(1,-1,0/1,1,0/0,0,2)$. The magnetic origin of some of the observed diffraction peaks was established by polarized neutron diffraction measurements. As in $YBa_2Fe_3O_8$, the iron moments are coupled antiferromagnetically within each (FeO_2) layer as well as along the c axis of the structure, and they lie in the planes perpendicular to c. The magnetic moments of the two iron atoms are practically identical and have values at room temperature of $\langle\mu\rangle=3.50(3)\mu_B$, $3.52(2)\mu_B$, and $3.62(2)\mu_B$ for the three compositions $x=0.05$, 0.10, and 0.20, respectively.

I. INTRODUCTION

The replacement of copper with iron in the superconductor $YBa_2Cu_3O_{6+\delta'}$ results in the compound of formula $YBa_2Fe_3O_{8+\delta}$. The structure of the latter material has been recently studied[1] in an attempt to detect possible correlations between structural modifications caused by the presence of iron and the lack of superconductivity. The atomic configurations of the copper and iron compounds differ mainly in the arrangement and the number of the oxygen atoms on the basal plane of the unit cell. In the 1:2:3 superconductor, when the oxygen stoichiometry corresponds to $\delta'=1$, the Cu atoms have square planar coordination and the Cu-O_2 units form the well-known chains that propagate along the b axis of the unit cell. For $\delta'=0$ these atoms become twofold coordinated and the compound is not superconducting. In the nonsuperconducting iron compound, the iron atoms of the basal plane have octahedral coordination[1] and the oxygen stoichiometry $8+\delta$ varies only over a narrow range $(-0.2<\delta<+0.1)$.[2] An important structural problem in this connection is to identify the location of the excess oxygen above 8. In this respect, the Ca substitution for Y has been used to influence the saturated oxygen content in a controlled manner.

Several investigations of the cuprates $(Y_{1-x}Ca_x)Ba_2Cu_3O_{6+\delta'}$, $(Y_{1-x}Ca_x)Ba_2Cu_4O_8$, and $(Y,Ca)(Ba,Sr)_2Cu_3O_{6+\delta'}$ have shown that replacing Y(III) with Ca(II) changes the electronic properties of the compounds in which the substitution occurs. In $(Y_{1-x}Ca_x)Ba_2Cu_3O_{6+\delta'}$ with $\delta'\approx 0.1$, for example, this substitution induces superconductivity up to a value of

TABLE I. Composition and x-ray powder-diffraction unit-cell parameters of $(Y_{1-x}Ca_x)Ba_2Fe_3O_{8+\delta}$.

Formula	v_{Fe}[a]	a (Å)	c (Å)
$(Y_{0.95}Ca_{0.05})Ba_2Fe_3O_{8.08(1)}$	3.068(5)	3.9175(5)	11.8093(40)
$(Y_{0.90}Ca_{0.10})Ba_2Fe_3O_{8.05(1)}$	3.069(5)	3.9188(6)	11.7889(17)
$(Y_{0.80}Ca_{0.20})Ba_2Fe_3O_{8.00(1)}$	3.064(5)	3.9114(4)	11.7660(14)

[a]Determined by cerimetric titration.

T_c of 44 K and structural refinements based on x-ray- and neutron-powder-diffraction data have shown that the Ca doping causes oxidation of the Cu atoms of the (CuO_2) layers, leaving the copper valence of the "chain" sites unchanged.[3,4] An increase of T_c from 80 to 90 K was also observed in the system $(Y_{1-x}Ca_x)Ba_2Cu_4O_8$ for $x=0.1$,[5] and also in this case we may presume that the oxidation affects only the copper atoms of the (CuO_2) layers. When doping by Ca is compensated by a corresponding reduction in oxygen content, the value of T_c does not change significantly,[6,7] thus showing that the controlling factor in determining T_c in this type of superconductors is the formal average valence of copper.

In order to gain information about the precise structure of the copper-free analogues of the superconducting compounds and to understand why, of all the transition metals, copper seems to be essential for the high-T_c superconductivity, Ca-doped samples of formula $(Y_{1-x}Ca_x)Ba_2Fe_3O_{8+\delta}$ have been prepared and analyzed by neutron-powder-diffraction techniques. In particular, it is interesting to determine the mechanism by which the charge balance is maintained during Ca doping; i.e., if it is achieved by iron oxidation or by releasing oxygen, or both.

II. EXPERIMENTAL RESULTS

A. Synthesis and characterization

Samples of $(Y_{1-x}Ca_x)Ba_2Fe_3O_{8+\delta}$ ($x=0.05$, 0.10, and 0.20) were prepared from liquid-mixed citrate precursors as described for $YBa_2Fe_3O_8$ in Ref. 8. Powders of Y_2O_3, $BaCO_3$, and $CaCO_3$ and high-purity Fe were used as starting materials. The products of the reaction were checked by x-ray powder diffraction using a Guinier-Hägg camera, with Cu$K\alpha_1$ radiation and Si as an internal standard. The unit-cell parameters deduced by least-squares refinements are shown in Table I.

The oxygen content was determined cerimetrically, by titration of Fe^{2+} left after dissolution of the finely powdered sample in a specified volume of ~0.1 M Mohr's salt/3 M HCl solution. The sealed ampoule technique and an Ar atmosphere were used in order to prevent any air oxidation during the dissolution (80 °C, 5 min). The exact Fe^{2+} content in the used volume of Mohr's salt solution was obtained in a separate titration. The overall Fe content in the sample was determined in a third titration, after reducing all iron into Fe^{2+} by the well-known $SnCl_2$ technique. The third titration eliminates the possible systematic error introduced by the Ce^{4+} molarity. The reproducibility of the determination upon one sample batch is better than ±0.003 oxygens per $YBa_2Fe_3O_8$ formula, and less than ±0.01 among separately synthesized batches. The results of these analyses are given in Table I.

B. Neutron-powder diffraction

The neutron-powder-diffraction measurements were made using the high-resolution five-counter diffractometer at the reactor of the National Institute of Standards and Technology, with the experimental conditions given in Table II. Complete diffraction scans were obtained at room temperature for each sample. In addition, scans of the magnetic peaks were taken in order to measure the temperature dependence of the magnetic reflections. For these measurements the BT-2 triple-axis spectrometer, operated in a two-axis mode with a graphite monochromator, was employed. The coarser resolution and concomitant higher intensity allowed an improved signal-to-noise ratio on these well-separated magnetic peaks. Finally, polarized neutron measurements were made on the BT-2 triple-axis diffractometer on a few selected reflections to establish their magnetic origin with the same procedure described in Ref. 1. All refinements were carried out using the Rietveld method,[9] adapted to the multicounter diffractometer and modified to include the background parameters.[10] In these calculations, the peak shape was described by a Pearson function.

The first set of refinements was made assuming as a structural model the perovskitelike cell of $YBa_2Fe_3O_8$ and the symmetry of space group $P4/mmm$. A few

TABLE II. Collection of intensity data.

Monochromatic beam	220 reflection of a Cu monochromator
Wavelength	1.545(1) (Å)
Horizontal divergences	10′,20′,10′ of arc for the in-pile, monochromatic beam, and diffracted beam collimators, respectively
Sample container	Vanadium or aluminum can of about 10 mm diameter
2θ angular range	5°–120°, steps: 0.05°
Scattering amplitudes (10^{-12} cm)	b(Y)=0.775, b(Ba)=0.525, b(Ca)=0.490, b(Fe)=0.954, b(O)=0.581

TABLE III. Refined structural parameters of $(Y_{1-x}Ca_x)Ba_2Fe_3O_{8+\delta}$ ($x=0.05$, 0.10, and 0.20) at room temperature.

			$x=0.05$			$x=0.10$			$x=0.20$		
Chemical unit cell:			$a=3.9162(1)$ Å, $c=11.8048(4)$ Å			$a=3.9149(1)$ Å, $c=11.7921(3)$ Å			$a=3.9115(1)$ Å, $c=11.7684(3)$ Å		
Space group: $P4/mmm$, $z=1$			$V=181.05(2)$ Å^3			$V=180.73(2)$ Å^3			$V=180.05(2)$ Å^3		
Atom		Position	x,y,z	B (Å^2)	n	x,y,z	B (Å^2)	n	x,y,z	B (Å^2)	n
Y	1*d*	4/*mmm*	$\frac{1}{2},\frac{1}{2},\frac{1}{2}$	0.89(8)	0.95	$\frac{1}{2},\frac{1}{2},\frac{1}{2}$	0.84(7)	0.90	$\frac{1}{2},\frac{1}{2},\frac{1}{2}$	0.62(6)	0.80
Ca	1*d*	4/*mmm*	$\frac{1}{2},\frac{1}{2},\frac{1}{2}$	0.89(8)	0.05	$\frac{1}{2},\frac{1}{2},\frac{1}{2}$	0.84(7)	0.10	$\frac{1}{2},\frac{1}{2},\frac{1}{2}$	0.62(6)	0.20
Ba	2*h*	4*mm*	$\frac{1}{2},\frac{1}{2},0.1658(4)$	0.63(6)	2	$\frac{1}{2},\frac{1}{2},0.1659(3)$	0.55(5)	2	$\frac{1}{2},\frac{1}{2},0.1661(3)$	0.74(5)	2
Fe(1)	1*a*	4/*mmm*	0,0,0	0.22(5)	1	0,0,0	0.32(4)	1	0,0,0	0.33(4)	1
Fe(2)	2*g*	4*mm*	0,0,0.3392(2)	0.66(4)	2	0,0,0.3395(2)	0.50(3)	2	0,0,0.3396(1)	0.50(3)	2
O(1)	2*g*	4*mm*	0,0,0.1817(3)	1.08(7)	2	0,0,0.1822(3)	0.99(6)	2	0,0,0.1832(3)	0.89(5)	2
O(2*A*)	4*i*	2*mm*.	$0,\frac{1}{2},0.3808(2)$	0.72(4)	3.66(2)	$0,\frac{1}{2},0.3790(2)$	0.68(4)	3.71(2)	$0,\frac{1}{2},0.3800(2)$	0.57(3)	3.88(2)
O(2*B*)	4*i*	2*mm*.	$0,\frac{1}{2},0.3400$	0.72(4)	0.34(2)	$0,\frac{1}{2},0.3400$	0.68(4)	0.29(2)	$0,\frac{1}{2},0.3400$	0.57(3)	0.12(2)
O(3)	2*f*	*mmm*.	$0,\frac{1}{2},0$	0.80(6)	2	$0,\frac{1}{2},0$	0.82(5)	2	$0,\frac{1}{2},0$	0.75(5)	2
O(4)	1*b*	4/*mmm*	$0,0,\frac{1}{2}$	1.00	0.085(5)	$0,0,\frac{1}{2}$	1.00	0.073(5)	$0,0,\frac{1}{2}$	1.00	0.029(5)
Magnetic unit cell:			$a=5.5384(1)$ Å, $b=5.5384(1)$ Å			$a=5.5365(1)$ Å, $b=5.5365(1)$ Å			$a=5.5317(1)$ Å, $b=5.5317(1)$ Å		
Orthorhombic, $z=4$			$c=23.6096(7)$ Å, $V=724.20(4)$ Å^3			$c=23.5842(6)$ Å, $V=722.92(3)$ Å^3			$c=23.5368(5)$ Å, $V=720.23(3)$ Å^3		
			$\mu_x=3.50(3)\mu_B$, $\mu_y=\mu_z=0\mu_B$			$\mu_x=3.52(2)\mu_B$, $\mu_y=\mu_z=0\mu_B$			$\mu_x=3.62(2)\mu_B$, $\mu_y=\mu_z=0\mu_B$		
Agreement factors			$R_{NM}=3.69(4.16)$[a], $R_N=3.67(4.12)$			$R_{NM}=3.22(3.67)$, $R_N=3.17(3.61)$			$R_{NM}=2.47(2.68)$, $R_N=2.38(2.64)$		
			$R_M=3.86(4.50)$, $R_p=5.67(5.82)$			$R_M=3.79(4.35)$, $R_p=5.42(5.58)$			$R_M=3.39(3.03)$, $R_p=4.63(4.64)$		
			$R_W=7.47(7.68)$ $\chi=1.29(1.33)$			$R_W=7.12(7.31)$, $\chi=1.24(1.27)$			$R_W=6.32(6.36)$, $\chi=1.33(1.34)$		

[a]The R factors for a model without the extra oxygen O(4) are indicated in parentheses.

peaks in the low-angle region of 2θ (5°–60°), could not be indexed on the unit cell determined by x rays. The structural similarity with $YBa_2Fe_3O_8$ suggested that these peaks could be attributed to magnetic ordering of the iron as in $YBa_2Fe_3O_8$. Polarized neutron-scattering measurements confirmed the magnetic origin of the peaks. The last set of refinements was carried out with a model for the antiferromagnetic structure identical to that described in Ref. 1 and using as initial nuclear structural parameters those refined previously. The magnetic form factor for iron was taken from Ref. 11. We also attempted to locate the oxygen in excess of the eight atoms per formula unit determined in the chemical analyses mentioned previously. Crystal chemical considerations suggest that the only sites available for such oxygen are those in the Y layer at $0,0,\frac{1}{2}$, assigned as O(4). Difference Fourier maps of the three samples were, in fact, consistent with the possible presence of extra nuclear density

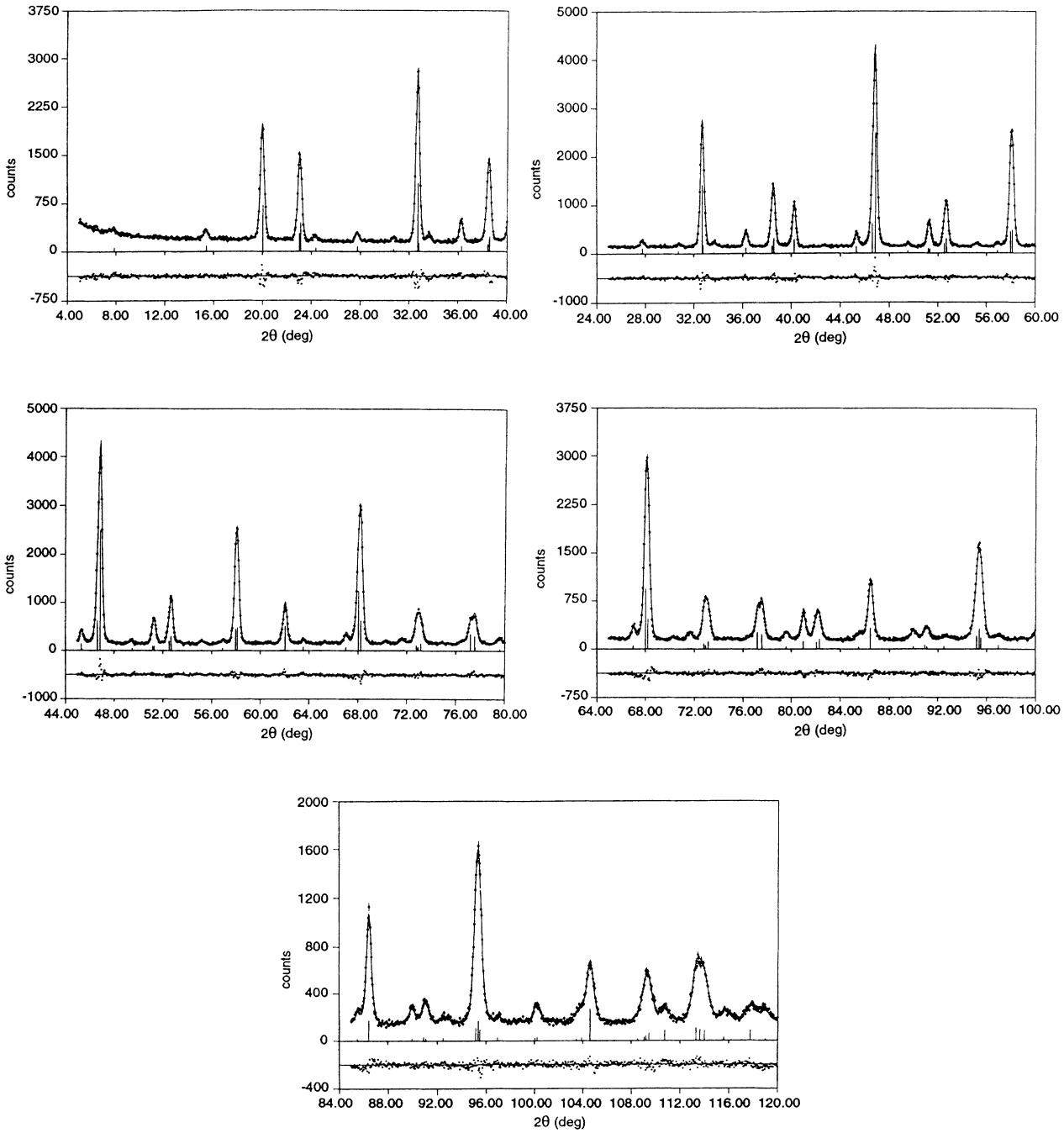

FIG. 1. Observed (circles) and calculated (continuous line) intensities in the neutron powder pattern of $(Y_{0.95}Ca_{0.05})Ba_2Fe_3O_{8.08(1)}$, for each of the five counters of the diffractometer. The differences between observed and calculated intensities are plotted at the bottom of each diagram. Similar results were obtained for the $x = 0.10$ and 0.20 samples.

at these locations. Refinements were therefore carried out in which the occupancy factors of the extra oxygen O(4) were varied while the temperature factor was kept fixed at a reasonable value. The values of the occupancies thus obtained were slightly larger than the results of the chemical analysis. This discrepancy is not significant and is quite probably due to the fact that the temperature factor of the O(4) atoms was arbitrarily fixed and could not be refined together with the occupancy parameter of these atoms. The introduction of O(4) into the structure improved the agreement between observed and calculated intensities, and as expected, the values in Table III show that the R factors improve most for the sample with the highest content of extra oxygen. The presence of the extra oxygen O(4) on the Y/Ca layer produces a certain disorder in the structure, reflected by a high-temperature factor (1.2 Å^2) of the oxygen atoms O(2) located near the plane of the iron atoms Fe(2) having pyramidal coordination. In those unit cells in which the sites O(4) are occupied, the oxygen atoms O(2) must be shifted towards the plane of the Fe(2) atoms in order to achieve a reasonable oxygen-oxygen distance and an octahedral coordination as regular as possible for Fe(2). On the other hand, when the sites O(4) are vacant, the atoms O(2) must be shifted away from the Fe(2) plane to ensure a stable pyramidal coordination for Fe(2). On the basis of these considerations, in the last refinements the atoms O(2) were located over two positions O(2A) and O(2B) with the following constraints: (i) the occupancies of O(2A) and O(2B) are such that n(O2A)+n(O2B)=4 and n(O2B)=4×n(O4); (ii) the oxygen-oxygen distances involved in the splitting assume reasonable values (>2.7 Å). Attempts to refine the z coordinates of O(2B) showed that these atoms were invariably located on the plane of the Fe(2) atoms. The parameters z(O2A) and z(O2B), however, were highly correlated with large values of the standard deviations and, for this reason, in the final refinement z(O2B) was kept fixed at a value practically identical with z(Fe2). The final nuclear and magnetic parameters obtained by simultaneous refinement are shown in Tables III and IV. Relevant interatomic distances are listed in Table V. The quality of the fit was excellent, with reduced $\chi^2=1.66$, as shown in Fig. 1 for $(Y_{0.95}Ca_{0.05})Ba_2Fe_3O_{8.08(1)}$.

The magnetic moments for both Fe sites were the same to within experimental error, and were therefore constrained to be equal in the final refinement. The room-temperature values obtained for $x=0.05$, 0.10, and 0.20 were $\langle\mu_x\rangle=3.50(3)\mu_B$, $3.52(2)\mu_B$, and $3.62(2)\mu_B$, respectively. The integrated intensities of the 103 reflection were measured over the temperature range $20<T<650$ K for the $x=0.05$ and 0.20 samples, whereas for the $x=0.10$ sample, this intensity was measured up to 675 K (see Fig. 2). Data for all samples were first collected above room temperature and then, about three months later, below room temperature. The two sets of data agree very well for the $x=0.05$ and 0.20 samples; however, for $x=0.10$, there is an obvious discrepancy between the high-temperature and low-temperature data. In order to check if structural changes had occurred for this composition, another complete neutron-powder-diffraction pattern was collected at room temperature. The refinement of this new pattern showed a contraction in the lattice parameters and an increase in the ordered magnetic moment, which indicated that changes had occurred, probably due to the fact that the $x=0.10$ sample had been heated to a higher temperature than the other two samples in the measurements above room temperature.

The variation of the 103 intensities for the $x=0.05$ and 0.20 samples over the entire temperature range, and the $x=0.10$ sample above room temperature, were fit to a mean-field model. The resulting fitted Néel temperatures are $T_N=638(2)$ K, $T_N=634(2)$ K, and $T_N=624(2)$ K for $x=0.05$, 0.10, and 0.20, respectively. Since the spin structure is collinear, the Fe moment increases with the square root of the 103 intensity. The measured low-temperature (10 K) Fe moments are therefore $3.90(10)\mu_B$ and $4.02(10)\mu_B$ for $x=0.05$ and 0.20. The $x=0.10$ low-temperature Fe moment is $3.95(10)\mu_B$ for the modified form of the sample. No low-temperature value

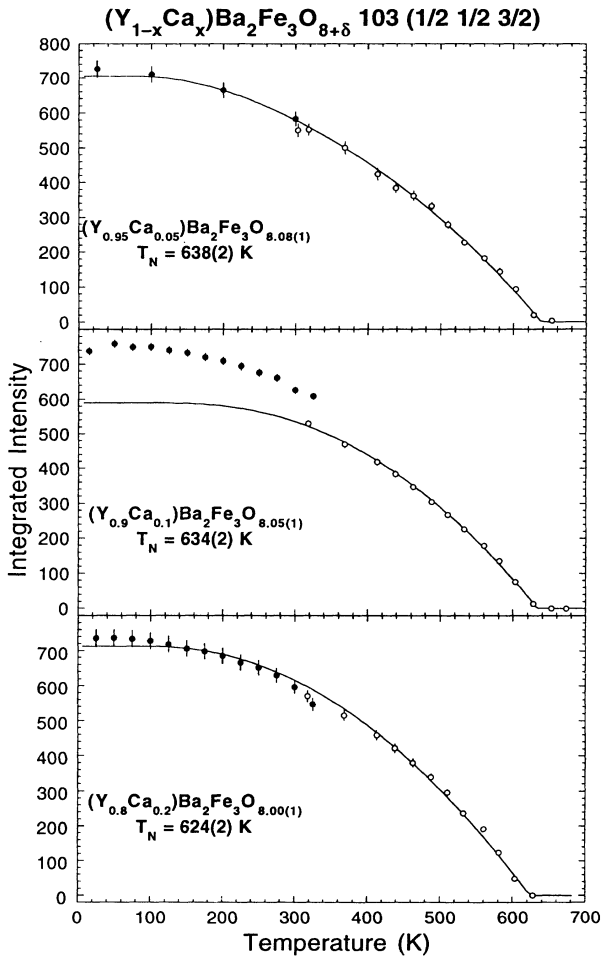

FIG. 2. Integrated intensities of the 103 reflection of $(Y_{0.95}Ca_{0.05})Ba_2Fe_3O_{8.08(1)}$, $(Y_{0.90}Ca_{0.10})Ba_2Fe_3O_{8.05(1)}$, and $(Y_{0.80}Ca_{0.20})Ba_2Fe_3O_{8.00(1)}$, respectively. The solid curves are fits of the square of a mean-field order parameter to the data. The discrepancy between the high- and low-temperature data for the $x=0.10$ sample is discussed in the text.

TABLE IV. Refined structural parameters of $(Y_{1-x}Ca_x)Ba_2Fe_3O_{8+\delta}$ for $x=0.10$ at room temperature after heating at 675 K.

Chemical unit cell:			$a=3.9136(1)$ Å, $c=11.7903(4)$ Å		
Space group: $P4/mmm, z=1$			$V=180.58(2)$ Å^3		
Atom	Position		x,y,z	B (Å^2)	n
Y	1*d*	4/*mmm*	$\frac{1}{2},\frac{1}{2},\frac{1}{2}$	0.83(6)	0.90
Ca	1*d*	4/*mmm*	$\frac{1}{2},\frac{1}{2},\frac{1}{2}$	0.83(6)	0.10
Ba	2*h*	4*mm*	$\frac{1}{2},\frac{1}{2}$,0.1659(3)	0.71(5)	2
Fe(1)	1*a*	4/*mmm*	0,0,0	0.43(4)	1
Fe(2)	2*g*	4*mm*	0,0,0.3395(2)	0.59(3)	2
O(1)	2*g*	4*mm*	0,0,0.1826(3)	0.89(6)	2
O(2*A*)	4*i*	2*mm*.	0,$\frac{1}{2}$,0.3812(2)	0.69(4)	3.72(2)
O(2*B*)	4*i*	2*mm*.	0,$\frac{1}{2}$,0.3400	0.69(4)	0.28(2)
O(3)	2*f*	*mmm*.	0,$\frac{1}{2}$,0	1.02(5)	2
O(4)	1*b*	4/*mmm*	0,0,$\frac{1}{2}$	1.00	0.071(5)
Magnetic unit cell:			$a=5.5346(1)$ Å, $b=5.5346(1)$ Å		
Orthorhombic, $z=4$			$c=23.5806(7)$ Å, $V=722.32(3)$ Å^3		
			$\mu_x=3.62(2)\mu_B$, $\mu_y=\mu_z=0\mu_B$		
Agreement factors			$R_{NM}=2.97(3.37)$[a], $R_N=2.82(3.21)$		
			$R_M=4.33(4.80)$, $R_P=5.48(5.60)$		
			$R_W=7.44(7.60)$, $\chi=1.29(1.31)$		

[a]The *R* factors indicated in parentheses refer to a model without the extra oxygen O(4).

is available for the $x=0.10$ sample in its original form, since extrapolating from the high-temperature data gives an artificially small value of the low-temperature moment (see Fig. 2), as has been seen by extrapolating fits of the high-temperature data from the other two samples.

III. DISCUSSION

The three samples of $(Y_{1-x}Ca_x)Ba_2Fe_3O_{8+\delta}$ have the same basic structure of $YBa_2Fe_3O_8$ (Ref. 1) as shown in

TABLE V. Selected interatomic distances (Å) in $(Y_{1-x}Ca_x)Ba_2Fe_3O_{8+\delta}$ at room temperature.

	$x=0.05$	$x=0.10$	$x=0.20$
Fe(1)-O(1)	2.144(6)	2.148(3)	2.156(3)
Fe(1)-O(3)	1.9581(1)	1.9574(1)	1.9558(1)
Fe(2)-O(1)	1.860(5)	1.855(4)	1.840(4)
Fe(2)-O(2*A*)	2.0187(8)	2.0171(7)	2.0128(6)
Fe(2)-O(2*B*)	1.9582(1)	1.9575(1)	1.9558(1)
Fe(2)-O(4)	1.898(2)	1.893(2)	1.888(2)
Ba-O(1)	2.7756(5)	2.7749(4)	2.7732(4)
Ba-O(2*A*)	3.206(4)	3.202(3)	3.188(3)
Ba-O(2*B*)	2.840(4)	2.837(3)	2.831(3)
Ba-O(3)	2.768(3)	2.767(3)	2.765(3)
Y/Ca-O(2*A*)	2.411(2)	2.410(1)	2.412(1)
Y/Ca-O(2*B*)	2.7206(1)	2.7187(1)	2.7149(1)
Y/Ca-O(4)	2.7692(1)	2.7682(1)	2.7659(1)
O(2*B*)-O(1)	2.707(3)	2.701(2)	2.689(2)
O(2*B*)-O(4)	2.7206(1)	2.7187(1)	2.7149(1)

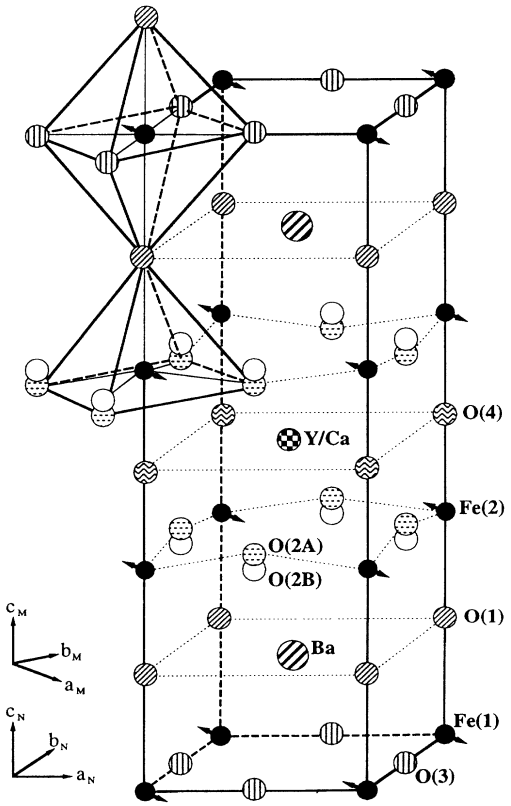

FIG. 3. Unit cell of $(Y_{1-x}Ca_x)Ba_2Fe_3O_{8+\delta}$. The magnetic cell is obtained from that of the figure by means of the axes transformation $(1,-1,0/1,1,0/0,0,2)$.

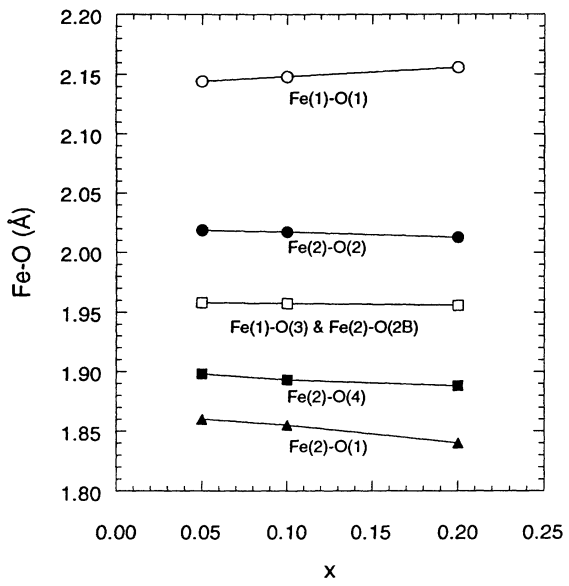

FIG. 4. Variation in Fe-O distances of $(Y_{1-x}Ca_x)Ba_2Fe_3O_{8+\delta}$ with Ca content between 0.05 and 0.20. The decrease in Fe-O distance is consistent with a constant Fe valence on Ca doping. For data on $x=0$, $\delta\approx 0$, see Ref. 1.

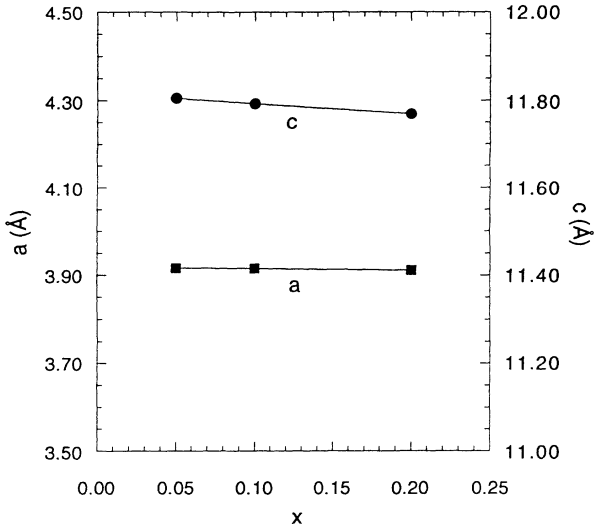

FIG. 5. Variation in unit-cell parameters of $(Y_{1-x}Ca_x)Ba_2Fe_3O_{8+\delta}$ with Ca content between 0.05 and 0.20. The decrease in the c-axis parameter is consistent with a loss of excess O from the Y/Ca plane on Ca doping, whereas the decrease in a is consistent with the Fe-O distance decrease shown in Fig. 4. For data on $x=0$, $\delta\approx 0$, see Ref. 1.

Fig. 3. The Ca and Y atoms are randomly distributed over the positions at $\frac{1}{2},\frac{1}{2},\frac{1}{2}$ and have eightfold prismatic coordination. The average Y/Ca-O bond distance slightly decreases as the Ca content increases. The barium atoms have 12 neighboring oxygen atoms forming a cuboctahedron and the average Ba-O bond lengths remain approximately constant as x increases.

There are two principal ways to achieve charge compensation for Ca doping: increase the Fe oxidation while the oxygen content is kept constant, or release oxygen while maintaining the Fe valence. As shown in Table I, the chemical analyses confirm that the Fe valence is maintained upon Ca doping, indicating the gradual disappearance of extra oxygen for the Ca-substituted samples. This variation in oxygen content is sufficient to balance the charge variation induced by Ca. The iron atoms are located on two symmetrically independent sites, Fe(1) and Fe(2), the first with octahedral and the second with square pyramidal coordination. The atoms Fe(2) are surrounded by 5.08, 5.05, and 5.00 oxygen atoms in the three compounds with $x=0.05$, 0.10, and 0.20, respectively. When the oxygen content decreases (i.e., when the Ca-doping increases), the average Fe(2)-O distance decreases. Bond-length, bond-strength calculations carried out using the formalism and the parameters given by Brown and Altermatt[12,13] give constant Fe(2) valences of +2.81 v.u. for the three samples. Thus, the effect of the loss of oxygen on the charge of the Fe(2) atom is compensated by the observed shortening of the bond distances of the oxygen atoms around Fe(2). Similar calculations for the octahedrally coordinated iron atoms Fe(1) give a constant valence of +3.01 v.u. for the three structures: the increase of the Fe(1)-O(1) distance from 2.144(6) to 2.156(3) Å in going from $x=0.05$ to 0.20 is compensated by a corresponding decrease of the Fe(1)-O(3) distance from 1.9581(1) to 1.9558(1) Å (Fig. 4). It appears, therefore, that the charge balance mechanism in the three cases examined in this study does not involve the iron atoms and that the effect of the substitution of Y^{3+} with Ca^{2+} is totally compensated by loss of oxygen. These results are in agreement with titration measurements which show no change in the total charge of iron.

The variation of the lattice parameters as function of the Ca doping is consistent with our interpretation that Ca^{2+} doping is compensated by oxygen loss alone (see Fig. 5). As the Ca content increases, the a parameter decreases, consistently with the shortening of the Fe(2)-O(2) and Fe(1)-O(3) bond distances, whereas the contraction of the c parameter can be attributed to the loss of oxygen in the Y/Ca planes.

As shown in Fig. 3, the magnetic structure of $(Y_{1-x}Ca_x)Ba_2Fe_3O_{8+\delta}$ is the same as that of $YBa_2Fe_3O_8$, described in Ref. 1, with the iron atoms coupled antiferromagnetically within each layer as well as along the c axis and with the magnetic moments lying in the planes perpendicular to c. This configuration gives an I-centered magnetic unit cell related to the nuclear cell by the transformation of the axes $(1,-1,0/1,1,0/0,0,2)$ and, as a consequence, all the magnetic reflections have half-integral indices when expressed in terms of the nuclear unit cell.

*Author to whom correspondence should be addressed.

[1]Q. Huang, P. Karen, V. L. Karen, A. Kjekshus, J. W. Lynn, A. D. Mighell, N. Rosov, and A. Santoro, Phys. Rev. B **45**, 9611 (1992).

[2]Q. Huang, P. Karen, V. L. Karen, A. Kjekshus, J. W. Lynn, A. D. Mighell, I. Natali Sora, N. Rosov, and A. Santoro (unpublished).

[3]E. M. McCarron, III, M. K. Crawford, and J. B. Parise, J. Solid State Chem. **78**, 192 (1989).

[4]J. B. Parise and E. M. McCarron III, J. Solid State Chem. **83**, 188 (1989).

[5]T. Miyatake, S. Gotoh, N. Koshizuka, and S. Tanaka, Nature **341**, 41 (1989).

[6]D. E. Morris, P. K. Narwankar, and A. P. B. Sinha, Physica C **169**, 7 (1990).

[7]M. R. Chandrachood, I. S. Mulla, S. M. Gorwadkar, and P. B. Sinha, Appl. Phys. Lett. **56**, 183 (1990).

[8]P. Karen, P. H. Andresen, and A. Kjekshus, J. Solid State Chem. **101**, 48 (1992).

[9]H. M. Rietveld, J. Appl. Crystallogr. **2**, 65 (1969).

[10]E. Prince, Natl. Bur. Stand. (U.S.) Tech. Note No. 1117, edited by F. J. Shorten (U.S. GPO, Washington, D.C., 1980), p. 8.

[11]J. H. Wood and G. W. Pratt, Phys. Rev. **107**, 995 (1957).

[12]I. D. Brown, *Structure and Bonding in Crystals* (Academic, New York, 1981), Vol. II, pp. 1–30.

[13]I. D. Brown, Phys. Chem. Minerals **15**, 30 (1987).